^{95}Mo NMR Studies of (Aryldiazenido)- and (Organohydrazido)molybdates. Crystal and Molecular Structure of [*n*-Bu₄N]₃[Mo₆O₁₈(NNC₆F₅)]

Shelton Bank,*,† Shuncheng Liu,† Shahid N. Shaikh,† Xiao Sun,† Jon Zubieta,*,† and Paul D. Ellis*,‡

The ^{95}Mo NMR spectroscopy of a select series of (aryldiazenido)- and (organohydrazido)molybdates of known structure has been studied. The chemical shifts, line widths, and in select cases T_1 values and the effects of temperature variation are reported. For the most part, with notable exceptions, the expected number of molybdenum signals are observed in the ^{95}Mo NMR spectra although temperature variation may be required to reveal the signals. There is a lack of simple correlation between component structural units in a given compound and some consistent chemical shift value that could be ascribed to that unit. In particular the spectrum for [Mo₆O₁₈(NNAr)]³⁻ differs markedly from that of [Mo₆O₁₉]²⁻, although the compounds are the closest structural analogues. Accordingly, the details of the structure, electronic spectrum, and electrochemistry of [Mo₆O₁₈(NNAr)]³⁻ are presented. Although the geometry of [Mo₆O₁₈(NNAr)]³⁻ is grossly related to that of [Mo₆O₁₉]²⁻ by substitution of a diazenido unit for an oxo group, the detailed investigations establish significant differences in the electronic spectra, redox electrochemistry, and structural parameters. Crystal data for [*n*-Bu₄N]₃[Mo₆O₁₈(NNC₆F₅)]: orthorhombic space group *Pmcn*; *a* = 17.345 (5), *b* = 17.645 (3), *c* = 24.434 (7) Å; *V* = 7478.1 (12) Å³; *Z* = 4; structure solutions and refinement based on 3534 reflections ($F_o \geq 3\sigma(F_o)$) converged at *R* = 0.059.

Introduction

The use of ^{95}Mo NMR spectroscopy to provide patterns and characterize Mo(VI) species has been an active area in the past 6 years.[1-10] In general, systematic substitution in mononuclear species leads to monotonic and often understandable patterns of variation of chemical shift, line width, and relaxation times. In the specific case of poly oxomolybdates, a relatively narrow range of chemical shifts has been observed for structural types as diverse as [MoO₄]²⁻, [PMo₁₂O₄₀]³⁻, and [Mo₆O₁₉]²⁻, which have chemical shift values of 0, 25, and 122 ppm, respectively, as compared to a range of some 4000 ppm for mononuclear Mo(VI) complexes, depending upon the ligand type.

Although the coordination chemistry of poly oxomolybdates is a relatively recent development, a variety of poly oxomolybdate–ligand complexes have been synthesized and structurally characterized. As part of our investigation of the chemistry of poly oxomolybdates with organohydrazine ligands, we have demonstrated using ^{17}O NMR spectroscopy that the solid-state structures of these poly oxomolybdo–organohydrazido complexes are maintained in solution. In this paper, we report the results of an initial survey of the ^{95}Mo NMR spectra of a range of organohydrazido-derivatized poly oxomolybdates.

Since the hexanuclear diazenido cluster [Mo₆O₁₈(NNAr)]³⁻ represents the structural analogue closest to the parent poly oxomolybdate type, namely the hexanuclear core of [Mo₆O₁₉]²⁻ with diazenido substitution for a terminal oxo group, the solid-state structure, the electronic spectra, and the electrochemistry of this cluster are presented in some detail. Although [Mo₆O₁₈(NNAr)]³⁻ presents a geometry grossly similar to that of [Mo₆O₁₉]²⁻, the consequences of diazenido coordination at a single Mo center are to perturb not only the solid-state structure but also the electronic spectrum and consequently the redox characteristics.

Experimental Section

The ^{95}Mo NMR spectra were obtained on a Bruker 400 spectrometer at 20.076 MHz using a 10-mm VSP probe. The 90° pulse was determined as 50 μs by using a 2 M sodium molybdate solution in D₂O at pH 11, which was used as the external chemical shift standard. To reduce the effect of acoustic ringing, the PATT and the RIDE pulse sequences for artifact suppression were employed.[11] A satisfactorily flat base line over a 10-kHz region was obtained. Typical conditions are noted in the caption for Figure 1. The relaxation times were obtained by using a standard inversion recovery sequence in addition to the RIDE sequence.

The compounds [Bu₄N]₂[Mo₂O₇] (**1**),[12] [Bu₄N]₂[Mo₆O₁₉] (**2**),[13] [Bu₄N]₄[Mo₈O₂₆] (**3**),[14] [Bu₄N]₂[Mo₄O₁₀(OMe)₂(N₂Ph₂)₂] (**4**),[15] [Bu₄N]₂[Mo₄O₈(OMe)₂(NNPh)₄] (**5**),[16] [Bu₄N]₂[Mo₄O₁₀(OMe)₂-(N₂PhMe)₂] (**6**),[17] [Bu₄N]₂[Mo₄O₁₂(hydralazine)] (**7**),[18] [Bu₄N]₂-

[Mo₄O₁₀(OMe)₂(N₂Ph)₂] (**8**),[18] [MePPh₃]₂[Mo₈O₁₆(OMe)₆(N₂PhMe)₆] (**9**),[19] [Bu₄N]₃[Mo₆O₁₈(NNPh)] (**10**),[20] and [Bu₄N]₄[Mo₈O₂₀(NNPh)₆] (**11**)[21] were prepared as described in the indicated references. Solutions (0.05–0.20 M) in the solvent or solvent mixtures recorded in Table I were prepared immediately before the spectra were recorded.

Synthesis of [(*n*-C₄H₉)₄N]₃[Mo₆O₁₈(NNC₆F₅)]. Addition of an excess of (pentafluorophenyl)hydrazine (0.4 g, 2.0 mmol) to a solution of α-[*n*-Bu₄N]₄[Mo₈O₂₆] (2.2 g, 1.0 mmol), followed by vigorous stirring at room temperature for 12 h, resulted in a dark brown solution. After removal of solvent by rotary evaporation at 22 °C, the oily brown product was washed three times with anhydrous diethyl ether. Crystallization was effected from a DMF/methanol/diethyl ether mixture (1:1:2 by volume). Anal. Calcd for C₅₄H₁₀₈N₅F₅O₁₈Mo₆: C, 36.3; H, 6.09; N, 3.92. Found:

(1) Christensen, K. A.; Miller, P. E.; Rockway, T. W.; Enemark, J. H.; *Inorg. Chim. Acta* **1981**, *56*, L27.

(2) Minelli, M.; Enemark, J. H.; Wieghardt, K.; Hahn, M. *Inorg. Chem.* **1983**, *22*, 3952.

(3) (a) Gheller, S. F.; Hambley, T. W.; Traill, P. R.; Brownlee, R. T. C.; O'Connor, M. J.; Snow, M. R.; Wedd, A. G. *Aust. J. Chem.* **1982**, *35*, 2183. (b) Gheller, S. F.; Sidney, M.; Masters, A. F.; Brownless, R. T. C.; O'Connor, M. J.; Wedd, A. G. *Aust. J. Chem.* **1984**, *37*, 1825.

(4) Gheller, S. F.; Gazzana, P. A.; Masters, A. F.; Brownlee, R. T. C.; O'Connor, M. J.; Wedd, A. G.; Rodgers, J. R.; Snow, M. R. *Inorg. Chim. Acta* **1981**, *54*, L131.

(5) Alyea, E. C.; Topich, J. *Inorg. Chim. Acta* **1982**, *65*, L95.

(6) Minelli, M.; Hubbard, J. L.; Christensen, K. A.; Enemark, J. H. *Inorg. Chem.* **1983**, *22*, 2653.

(7) Buchanan, I.; Minelli, M.; Ashby, M. T.; King, T. J.; Enemark, J. H. *Inorg. Chem.* **1984**, *23*, 495.

(8) Minnelli, M.; Yamanouchi, K.; Enemark, J. H.; Subramanian, P.; Kaul, B. B.; Spence, J. T. *Inorg. Chem.* **1984**, *23*, 2554.

(9) Minelli, M.; Young, C. G.; Enemark, J. H. *Inorg. Chem.* **1985**, *24*, 1111.

(10) Brownlee, R. T. C.; O'Connor, M. J.; Shehan, B. P.; Wedd, A. G. *Aust. J. Chem.* **1986**, *39*, 931.

(11) (a) Patt, S. L. *J. Magn. Reson.* **1982**, *49*, 161. (b) Benesi, A. J.; Ellis, P. D., submitted for publication in *J. Magn. Reson.*

(12) Day, V. W.; Friedrich, M. F.; Klemperer, W. G.; Shum, W. *J. Am. Chem. Soc.* **1977**, *99*, 6146.

(13) (a) Che, M.; Fournier, M.; Launay, J. P. *J. Chem. Phys.* **1979**, *71*, 1954. (b) Dahlstrom, P.; Zubieta, J. A.; Neaves, B.; Dilworth, J. R. *Cryst. Struct. Commun.* **1982**, *11*, 463.

(14) (a) Fuchs, J.; Hartl, H. *Angew. Chem., Int. Ed. Engl.* **1976**, *15*, 375. (b) Filowitz, M.; Ho, R. K. C.; Klemperer, W. G.; Shum, W. *Inorg. Chem.* **1979**, *18*, 93.

(15) Shaikh, S. N.; Zubieta, J. A. *Inorg. Chem.* **1986**, *25*, 4613.

(16) (a) Hsieh, T. C.; Zubieta, J. A. *Polyhedron* **1986**, *5*, 305. (b) Hsieh, T. C.; Zubieta, J. A. *Inorg. Chem.* **1985**, *24*, 1287.

(17) See ref 15.

(18) Shaikh, S. N.; Zubieta, J. A. *Inorg. Chem.* **1988**, *27*, 1896.

(19) (a) Shaikh, S. N.; Zubieta, J. A. *Inorg. Chim. Acta* **1986**, *121*, L43. (b) Shaikh, S. N.; Zubieta, J. A. *Inorg. Chem.* **1987**, *26*, 4079.

(20) Hsieh, T.-C.; Zubieta, J. A. *Polyhedron* **1985**, *5*, 1655.

(21) Hsieh, T.-C.; Zubieta, J. A. *J. Chem. Soc., Chem. Commun.* **1985**, 1749.

† State University of New York at Albany.

‡ University of South Carolina.
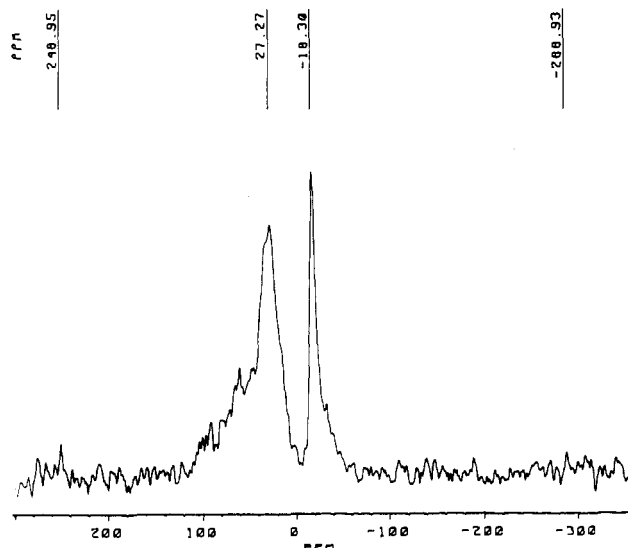
Figure 1. ^{95}Mo NMR spectra of $[Bu_4N]_2[Mo_4O_{10}(OMe)_2(N_2Ph_2)_2]$ (4) in CD_2Cl_2 and CH_3OH at 292 K after 116 243 transients with 50-Hz line broadening applied.

C, 36.0; H, 6.17; N, 3.82. IR (cm^{-1}, KBr pellet): ν(N=N), 1485 (s); ν(Mo—O$_t$), 945 (s); ν(Mo—O$_b$), 790 (m). UV/visible in acetonitrile [λ_{max}, nm (ϵ M^{-1} cm^{-1})]: 523 (2.7 × 10^4), 379 (1.3 × 10^5), 276 (1.5 × 10^5).

X-ray Crystallographic Study of $[(n\text{-}C_4H_9)_4N]_3[Mo_6O_{18}(NNC_6F_5)]$. The details of the crystal data, data collection methods, and refinement procedures are given in the supplementary material. Crystal data for $[n\text{-}Bu_4N]_3[Mo_6O_{18}(NNC_6F_5)]$: orthorhombic space group *Pmcn*; $a = 17.345$ (5), $b = 17.645$ (3), $c = 24.434$ (7) Å; $V = 7478.1$ (12) Å^3; $Z = 4$; structure solutions and refinement based on 3534 reflections ($F_o \geq 3\sigma(F_o)$) converged at $R = 0.059$. Full details of the crystallographic methodologies may be found.[22]

Although the complex anion was well-behaved in the refinement cycles, the tetrabutylammonium cations displayed some disorder, as suggested by a spread in the C–C distances, 1.32–1.64 Å, some large temperature factors, and a number of excursions of electron density on the order of 1.2 e/Å^3 on the final difference Fourier maps, associated with possible carbon positions. Since no disorder model provided a significant improvement over the simple expedient of locating the carbon positions at the largest peaks consistent with atom positions, no further attempt was made to introduce a disorder model into the final refinement cycles.
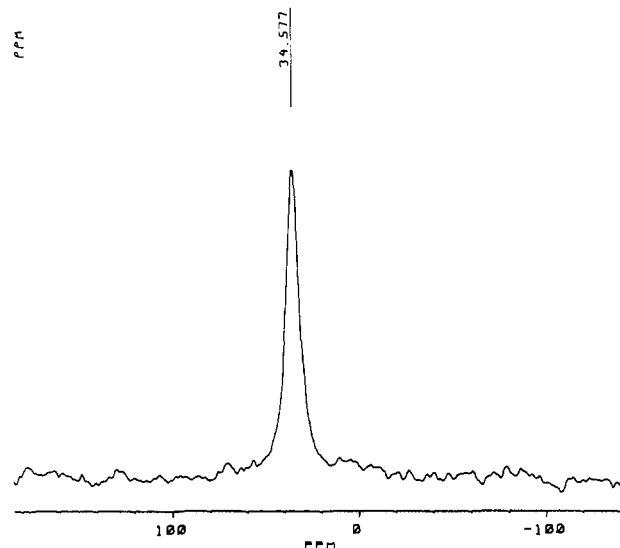
Electrochemical Measurements and Electron Paramagnetic Resonance Studies. Cyclic voltammograms were performed on a BAS-100 electrochemical analyzer at a complex concentration of 5 × 10^{-3} M in CH_2Cl_2 solution with 0.2 M [n-Bu$_4$N][PF$_6$] as supporting electrolyte. A Pt-bead working electrode, Ag-wire auxiliary electrode, and a Ag/AgCl reference electrode were employed in a conventional three-electrode configuration. All potentials were standardized with respect to the ferrocene/ferrocenium couple in CH_2Cl_2. Controlled-potential electrolyses were performed at a 0.5 cm per edge Pt-gauze electrode in acetonitrile solution 10^{-2} M in complex and 0.5 M in [n-Bu$_4$N][PF$_6$] supporting electrolyte.

Solutions for EPR measurements were taken directly from the electrolysis cell. EPR spectra were recorded on a Varian E-4 spectrometer at room temperature and at liquid-nitrogen temperature. Spectra at 10 K were recorded on a Bruker ER 200 spectrometer.

Results

The preparations and structural determinations of the molybdenum compounds are described in other publications. Solutions of the molybdenum compounds in the appropriate solvents were prepared, and spectra were taken as soon after mixing as possible as well as after periods of time. For many of the compounds spectra were recorded as a function of temperature, and the relaxation times (T_1) were obtained for one compound.

Figures 1–3 depict typical molybdenum spectra for representative compounds, and Tables I and II record the relevant ^{95}Mo NMR data for all the compounds of this study. The chemical shifts of $[Mo_6O_{19}]^{2-}$, $[Mo_8O_{26}]^{4-}$, and dimolybdate agree well with

(22) Bruce, A.; Corbin, J. L.; Dahlstrom, P. L.; Hyde, J. R.; Minelli, M.; Steifel, E. I.; Spence, J. T.; Zubieta, J. *Inorg. Chem.* **1982**, *21*, 917.

Figure 2. ^{95}Mo NMR spectra of $[Bu_4N]_2[Mo_4O_8(OMe)_2(NNPh)_4]$ (5) in CD_2Cl_2 at 292 K after 46 406 transients with 50-Hz line broadening applied.
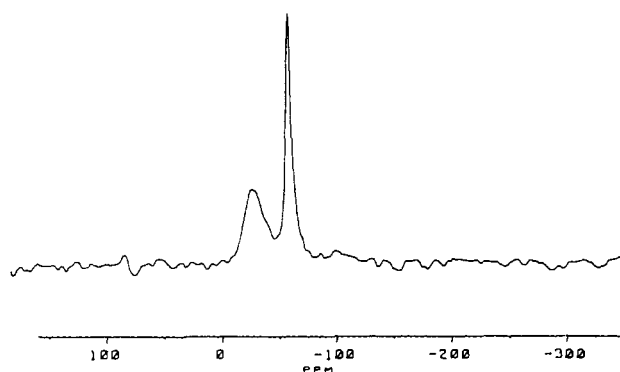
Figure 3. ^{95}Mo NMR spectra of $[Bu_4N]_4[Mo_8O_{20}(NNPh)_6]$ (11) in CD_2Cl_2 at 302 K after 100 263 transients with 50-Hz line broadening applied.

the values obtained by other workers.[3b] Figure 1 for compound **4** with one tetrahedral and one octahedral molybdenum site displays the expected two signals with considerable line width differences. The spectrum for compound **5** (Figure 2), on the other hand, with a similar distribution of octahedral and tetrahedral sites reveals only a single signal. The spectrum for compound **11** (Figure 3) displays two signals whereas the structure has three distinct Mo sites. Thus, while the number of ^{95}Mo NMR signals should be directly related to the number of unique Mo centers in the structure, occasionally the spectra obscure the simple relationship.

A notable example of the problem and its resolution is described for compound **3**. Figure 4 depicts the fully reversible temperature-dependent spectra of this compound. The spectrum of $[Mo_8O_{26}]^{4-}$ at 292 K has a single peak at 18.6 ppm. However, at 337 K two signals at 24.2 and −5.2 ppm, respectively, of differing line widths are clearly present. Thus, the temperature increase of 45 K has brought about a 6 ppm deshielding change in one signal and a sufficient narrowing of the other signal to allow observation. Relaxation studies of these signals reveal T_1 values of 22 and 0.5 ms, respectively. Accordingly, the absence of a signal at the lower temperature is the result of a very broad signal that is not distinguished from the noise.

The resonance with 41-Hz signal width is assigned to the tetrahedral molybdenum in accord with the greater symmetry at this site, and therefore, the ratio of intensities should be 1:3. Processing of spectra with signal widths of 41 and 463 Hz to provide accurate intensity ratios has some difficulties; nevertheless, under the best possible choices for applied line broadening the
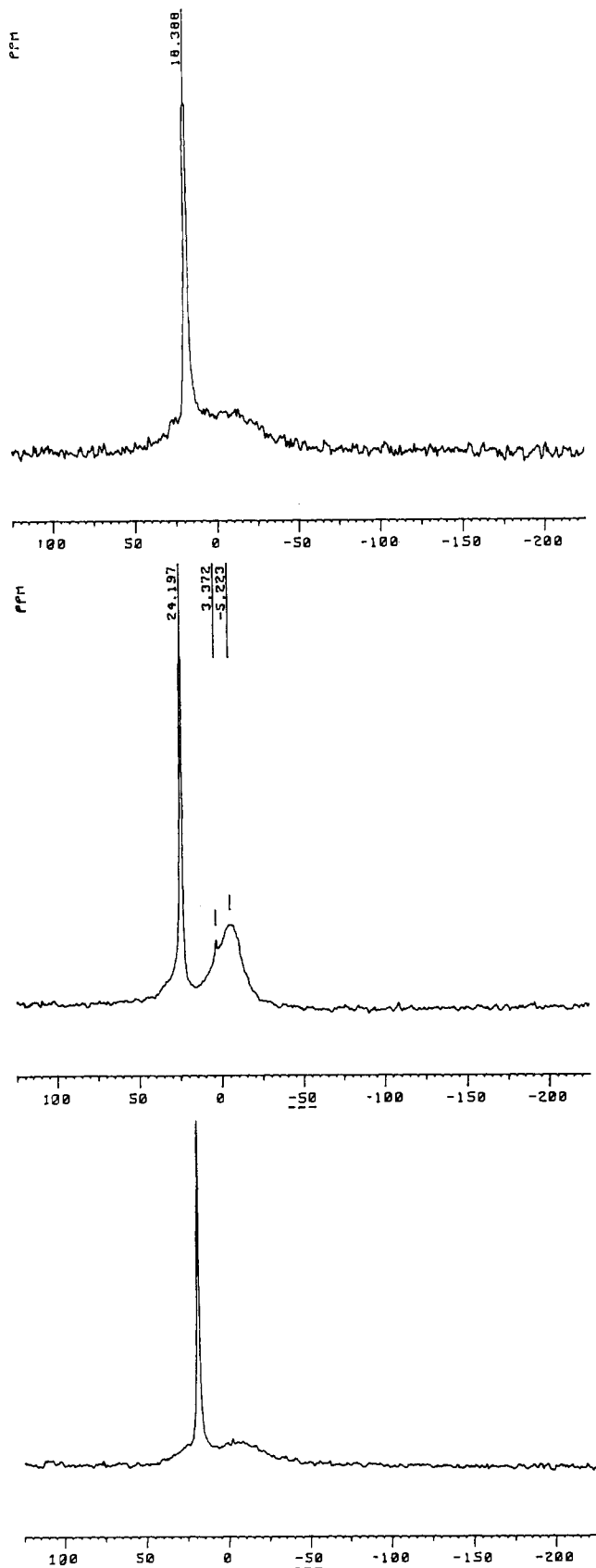
Figure 4. ^{95}Mo NMR spectra of $[Bu_4N]_4[Mo_8O_{26}]$ (3) in CD$_3$CN at (top) 292 K, (middle) 337 K (the spurious maximum at 3.372 ppm due to electronic noise), and (bottom) 292 K after heating.

Figure 5. ^{95}Mo NMR spectra $[Bu_4N)_3[Mo_6O_{18}(NNPh)]$ (10) in CD$_3$CN at (top) 292 K, and (bottom) 292 K after heating to 337 K.
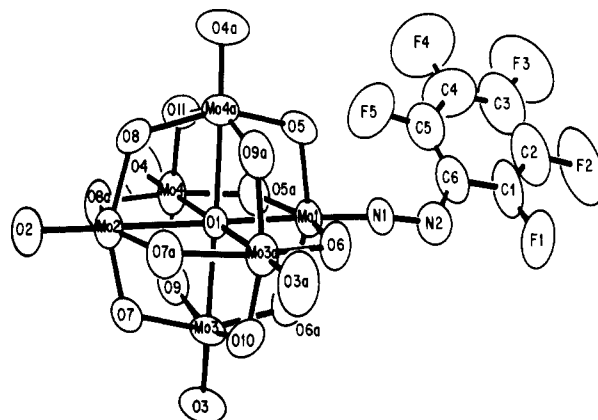
Figure 6. ORTEP view of the structure of $[Mo_6O_{18}(NNC_6F_5)]^{3-}$, showing the atom-labeling scheme.

ratio obtained was 1:2.6. Therefore, both the line widths and the intensities support the assignments.

Unfortunately, this strategy is not uniformly successful, as the spectra depicted in Figure 5 reveal. Whereas a single signal is observed at t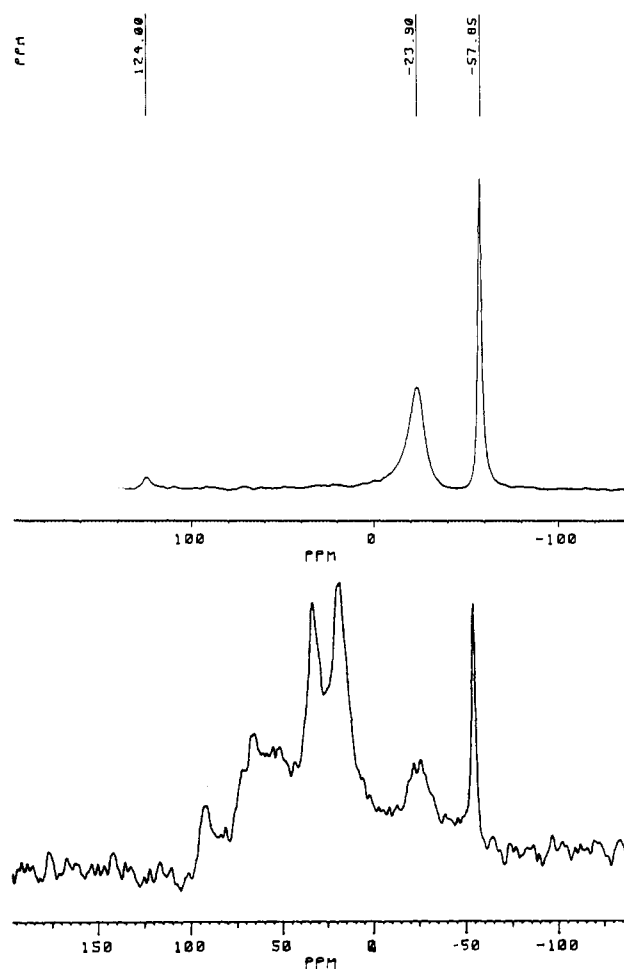he lower temperatures and additional signals are observed at 337 K (not shown), the spectrum at 292 K after heating has changed significantly from the original. Thus, the process is not reversible and unambiguous signal assignment is not possible in this case.
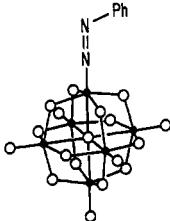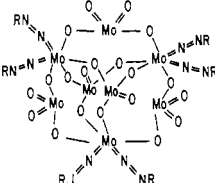
Structure of $[n\text{-}Bu_4N]_3[Mo_6O_{18}(NNC_6F_5)]$. Table III lists the crystallographic data for the structure, and atomic positional parameters are tabulated in Table IV. Table V presents selected bond lengths and angles for the structure of $[n\text{-}Bu_4N]_3$-$[Mo_6O_{18}(NNC_6F_5)]$.

As illustrated by Figure 6, the structure of the complex anion consists of discrete hexanuclear units incorporating a single coordinatively bound (pentafluorophenyl)diazenido group and containing a mirror plane passing through Mo(1), Mo(2), O(1), O(2), O(10), O(11), and the –NNC$_6$F$_5$ unit. This anion represents

Table I. ^{95}Mo Chemical Shifts for Molybdenum Complexes

compd no.	formula of anion	structure	tetra-hedral O_t	O_b	octahedral O_t	O_b	N_t	N_b	shifts,[b] ppm, and solvent	line width, Hz	temp effect[c]
1	$[Mo_2O_7]^{2-}$		3	1					−5.8 CD$_2$Cl$_2$	10	
2	$[Mo_6O_{19}]^{2-}$				1	5			126.0 DMF-d_7	70	reversible
3	$[Mo_8O_{26}]^{4-}$		1	3	2	4			24.2 −4.2 CD$_3$CN	41^d 463^e	reversible
4	$[Mo_4O_{10}(OMe)_2(N_2Ph_2)]^{2-}$		2	2	1	4	1		26.3 −17.5 CD$_2$Cl$_2$/CH$_3$OH	300 100	
5	$[Mo_4O_8(OMe)_2(N_4Ph)_4]^{2-}$		2	2		4	2		35.1 CD$_2$Cl$_2$	100	some minor decay
6	$[Mo_4O_{10}(OMe)_2(N_2MePh)_2]^{2-}$		2	2	1	4	1		25.0 −16.0 CD$_2$Cl$_2$/CH$_3$OH	300 100	
7	$[Mo_4O_{12}(hydralazine)]^{2-}$		2	2	2	3	1		25.0	200	reversible
					1	2	1	1	−16.0 CD$_2$Cl$_2$	100	
8	$[Mo_4O_{10}(OMe)_2(N_2Ph)_2]^{2-}$		2	2		4	2		−63.0	100	decays with time
					2	4			−24.0 35.5 CD$_2$Cl$_2$	300 300	
9	$[Mo_8O_{16}(OMe)_6(N_2MePh)_6]^{2-}$				1	5			60.0	700	
						5		1	CD$_2$Cl$_2$/CH$_3$OH		

Table I (Continued)

compd no.	formula of anion	structure	Mo sites[a]						shifts,[b] ppm, and solvent	line width, Hz	temp effect[c]
			tetra-hedral		octahedral						
			O_t	O_b	O_t	O_b	N_t	N_b			
10	$[Mo_6O_{18}(N_2Ph)]^{3-}$		1	5					−57.9	100	irreversible
			1	5					−23.9	500	
					5	1			CD_3CN		
11	$[Mo_8O_{20}(N_2Ph)_6]^{4-}$		2	2	4	2			−58.9	100	irreversible
			1	3					−27.5	500	
									CD_2Cl_2		

[a] Molybdenum sites to terminal (t) or bridging (b) oxygen or nitrogens. [b] Chemical shift at 292 K reference to external Na_2MoO_4 in D_2O at pH 11. [c] Behavior on heating to 327 ● 10 K and return to 292 K. [d] T_1 = 22.0 ms. [e] T_2 = 0.5 ms.

Table II. Chemical Shifts of Tetrahedral and Octahedral Molybdenum Sites for Poly Oxomolybdates of This Study

no. of Mo–O_t[a]	no. of Mo–O_b[b]	chem shift,[c] ppm	complex
		Tetrahedral Sites	
4	0	0.0	$[MoO_4]^-$
3	1	−5.8	1
2	2	−63.0	8
		−17.0	4, 6
		35.1	5
1	3	−60.0	11
		−26.0	11
		24.2	3
		Octahedral Sites	
1	5	−57.9	10
		−23.9	10
		60.0	9
		126.0	2
2	4	35.5	8(?)
		−4.2	3
		−24.0	8(?)

[a] Number of molybdenum sites to terminal oxygens. [b] Number of molybdenum sites to bridging oxygens. [c] Tentatively assigned possible or probable chemical shifts values referenced to external Na_2MoO_4 in D_2O at pH 11.

Table III. Crystallographic Data for $[n$-$Bu_4N]_3[Mo_6O_{18}(NNC_6F_5)]$

chem formula: $C_{54}H_{108}N_5F_5O_{18}Mo_6$	space group: *Pmcn*
fw: 1786.1	T = 296 K
a = 17.345 (5) Å	λ = 0.71073 Å
b = 17.645 (3) Å	ρ_{calcd} = 1.584 g cm^{-3}
c = 24.434 (7) Å	μ = 9.98 cm^{-1}
V = 7478.1 (12) Å^3	R = 0.059
Z = 4	R_w = 0.064

a modification of the well-known $[Mo_6O_{19}]^{2-}$ anion[23] in which a single terminal oxo group has been replaced by a (pentafluorophenyl)diazenido ligand while the structural integrity of the hexanuclear framework is maintained.

The geometry of the hexanuclear core of molybdenum atoms is distorted from the idealized octahedral symmetry displayed by
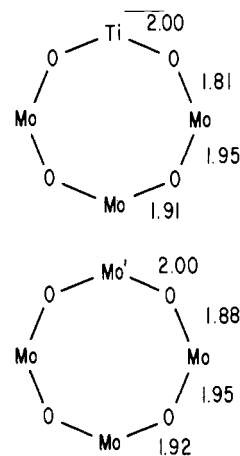
(23) Allcock, H. R.; Bissell, E. C.; Shawl, E. T. *Inorg. Chem.* **1973**, *12*, 2963. Garner, C. D.; Howlander, N. C.; Mabbs, F. E.; McPhail, A. T.; Miller, R. W.; Onan, K. D. *J. Chem. Soc., Dalton Trans.* **1978**, 1582. Nagano, O.; Saseki, Y. *Acta Crystallogr., Sect. B: Struct. Crystallogr. Cryst. Chem.* **1979**, *B35*, 2387. Dahlstrom, P.; Zubieta, J.; Neaves, B.; Dilworth, J. R. *Cryst. Struct. Commun.* **1982**, *11*, 463.

Figure 7. Comparison of bond lengths in the $TiMo_3O_4$ and $Mo(1)Mo_3O_4$ rings of $[(Mo_5O_{18})Ti(C_5H_5)]^{3-}$ and $[(Mo_5O_{18})Mo(NNC_6F_5)]^{3-}$, respectively.

$[Mo_6O_{19}]^{2-}$ as a consequence of phenyldiazenido substitution at Mo(1). The Mo(1)–O(1) distance is significantly shorter than the average of the Mo–O(1) bond distances, 2.19 (1) Å in contrast to 2.36 (1) Å (average). A concomitant effect is the shortening of the Mo(1)–Mo(3) and Mo(1)–Mo(4) distances to 3.233 (3) Å from an average Mo–Mo distance of 3.324 (4) Å for all other intermetal distances. The distortions presented by the Mo–bridging oxygen distances also reflect the consequences of replacing the Mo=O unit by the Mo=N—NR group. Thus, the Mo-(1)–O(5) and Mo(1)–O(6) distances are significantly longer than the Mo(3)–O(6a) and Mo(4)–O(5a) distances, 2.00 (1) Å (average) in contrast to 1.88 (1) Å (average), while the average Mo–bridging oxygen distance for all other bonds of this type is 1.94 (2) Å. Although systematic variation of bond lengths in the $[Mo_6O_{18}(NNC_6F_5)]^{3-}$ structure is difficult to establish due to the relatively low precision of the structure determination, the pattern of bond length distortions is similar to that observed for the $[(C_5H_5)TiMo_5O_{18}]^{3-}$ structure, where short–long bond length alternation is clearly evident in each $[TiMo_3O_4]$ ring,[24] as shown in Figure 7. The pattern observed for $[Mo_6O_{18}(NNC_6F_5)]^{3-}$ is also systematic and results from the replacement of the $[Mo^{VI}O_t]^{4+}$ unit in $[Mo_6O_{19}]^{2-}$ with the trivalent $[Mo^{II}NNC_6F_5)]^{3+}$ unit. As

(24) Che, T. M.; Day, V. W.; Francesconi, L. C.; Fredrich, M. F.; Klemperer, W. G.; Shum, W. *Inorg. Chem.* **1985**, *24*, 4055.

Table IV. Atomic Coordinates ($\times 10^4$) and Equivalent Isotropic Displacement Parameters ($\text{Å}^2 \times 10^3$) for [n-Bu$_4$N]$_3$[Mo$_6$O$_{18}$(NNC$_6$F$_5$)]

	x	y	z	U(eq),^{a} Å^2
Mo(1)	2500	5573 (1)	2122 (1)	45 (1)
Mo(2)	2500	7860 (1)	2987 (1)	53 (1)
Mo(3)	1540 (1)	6250 (1)	3147 (1)	59 (1)
Mo(4)	1540 (1)	7121 (1)	1941 (1)	60 (1)
O(1)	2500	6669 (8)	2542 (6)	39 (5)
O(2)	2500	8716 (10)	3297 (8)	77 (8)
O(3)	878 (9)	5946 (8)	3606 (6)	97 (6)
O(4)	873 (9)	7459 (9)	1505 (6)	97 (6)
O(5)	3297 (7)	6128 (6)	1693 (4)	58 (4)
O(6)	3298 (7)	5395 (6)	2703 (5)	63 (5)
O(7)	1742 (7)	7284 (6)	3387 (5)	60 (4)
O(8)	3261 (8)	7970 (6)	2425 (5)	68 (5)
O(9)	955 (6)	6714 (7)	2551 (5)	71 (5)
O(10)	2500	5999 (9)	3512 (7)	69 (7)
O(11)	2500	7416 (10)	1582 (7)	62 (7)
N(1)	2500	4693 (11)	1796 (8)	50 (7)
N(2)	2500	3994 (14)	1634 (12)	88 (12)
F(1)	2500	2534 (11)	1350 (13)	95 (13)
F(2)	2500	2041 (15)	333 (13)	102 (17)
F(3)	2500	3069 (22)	−551 (13)	98 (24)
F(4)	2500	4533 (18)	−300 (12)	110 (23)
F(5)	2500	5042 (12)	722 (8)	122 (13)
C(1)	2500	3043 (20)	911 (21)	81 (9)
C(2)	2500	2824 (31)	405 (29)	78 (31)
C(3)	2500	3348 (42)	−34 (26)	71 (36)
C(4)	2500	4043 (29)	115 (18)	89 (31)
C(5)	2500	4314 (22)	644 (15)	86 (16)
C(6)	2500	3848 (17)	1079 (15)	60 (12)
N(3)	4962 (10)	4184 (9)	1873 (6)	69 (4)
N(4)	2500	8743 (17)	223 (12)	96 (9)
C(7)	5253 (12)	3519 (11)	1523 (8)	73 (6)
C(8)	4607 (13)	3139 (13)	1184 (9)	91 (7)
C(9)	4938 (16)	2497 (16)	868 (11)	126 (10)
C(10)	4372 (19)	2053 (17)	546 (13)	170 (14)
C(11)	4654 (13)	4820 (12)	1493 (9)	87 (7)
C(12)	5196 (14)	5155 (13)	1105 (9)	92 (7)
C(13)	4760 (16)	5728 (16)	751 (11)	125 (10)
C(14)	5220 (21)	6112 (20)	412 (14)	216 (19)
C(15)	5658 (12)	4447 (12)	2198 (9)	83 (6)
C(16)	5576 (15)	5129 (14)	2565 (10)	108 (8)
C(17)	6326 (20)	5380 (19)	2836 (14)	172 (14)
C(18)	6314 (31)	5955 (26)	3191 (19)	150 (24)
C(19)	4310 (12)	3955 (11)	2264 (8)	75 (6)
C(20)	4476 (13)	3306 (13)	2648 (9)	92 (7)
C(21)	3720 (18)	3076 (17)	2955 (12)	147 (12)
C(22)	3752 (21)	2453 (20)	3328 (14)	207 (18)
C(23)	2500	8027 (20)	−73 (15)	140 (16)
C(24)	2500	7296 (25)	95 (19)	144 (23)
C(25)	2500	6480 (21)	−194 (17)	98 (24)
C(26)	2500	5701 (22)	−227 (16)	65 (27)
C(27)	2500	9360 (21)	−215 (16)	149 (17)
C(28)	2500	10115 (20)	−16 (15)	90 (26)
C(29)	2500	10828 (21)	−230 (15)	99 (21)
C(30)	2500	11552 (22)	−524 (17)	151 (25)
C(31)	3284 (14)	8849 (17)	510 (10)	129 (10)
C(32)	4156 (12)	8920 (18)	491 (22)	180 (29)
C(33)	4606 (17)	8885 (21)	757 (23)	211 (22)
C(34)	5026 (18)	9514 (20)	825 (24)	129 (25)

^{a} Equivalent isotropic U defined as one-third of the trace of the orthogonalized U$_{ij}$ tensor.

anticipated, Mo–O(bridging) bonds for the formally Mo(II) center (Mo(1)) are significantly weaker than those for the Mo(VI) centers (Mo(2)–Mo(4a)). Thus, the Mo(3)–O(bridging) and Mo(4)–O(bridging) bonds are short, and the bonds trans to these are weakened, resulting in the concomitant shortening of the Mo(2)–O(bridging) bonds. The trans character of this bond alternation has been described in terms of a classical off-center displacement[24,25] of metals in a rigid, close-packed oxygen framework. In fact, the structure of [Mo$_6$O$_{18}$(NNC$_6$F$_5$)]$^{3-}$ may

(25) Megaw, H. D. *Acta Crystallogr., Sect. B: Struct. Crystallogr. Cryst. Chem.* **1968**, *B24*, 149.

Table V. Selected Bond Lengths (Å) and Angles (deg) for [n-Bu$_4$N]$_3$[Mo$_6$O$_{18}$(NNC$_6$F$_5$)]

Mo(1)–O(1)	2.19 (1)		
Mo(1)–O(5)	1.99 (1)	Mo(3)–O(9)	1.96 (1)
Mo(1)–O(6)	2.01 (1)	Mo(3)–O(10)	1.94 (1)
Mo(1)–N(1)	1.75 (2)	Mo(3)–O(1)	2.35 (1)
Mo(2)–O(1)	2.37 (1)	Mo(3)–O(3)	1.69 (1)
Mo(2)–O(2)	1.69 (1)	Mo(4)–O(1)	2.36 (1)
Mo(2)–O(7)	1.93 (1)	Mo(4)–O(4)	1.68 (1)
Mo(2)–O(8)	1.91 (1)	Mo(4)–O(9)	1.94 (1)
N(1)–N(2)	1.30 (3)	Mo(4)–O(11)	1.95 (1)
Mo(3)–O(6a)	1.88 (1)	Mo(4)–O(5a)	1.88 (1)
Mo(3)–O(7)	1.95 (1)	Mo(4)–O(8a)	1.94 (1)
Mo(1)··Mo(3)	3.236 (2)	Mo(3)··Mo(4)	3.325 (2)
Mo(1)··Mo(4)	3.229 (2)	Mo(3)··Mo(3a)	3.329 (2)
Mo(2)··Mo(3)	3.316 (2)	Mo(4)··Mo(4a)	3.331 (2)
Mo(2)··Mo(4)	3.317 (2)		

Mo(1)–N(1)–N(2)	170.6 (21)	Mo(2)–O(7)–Mo(3)	117.5 (5)
Mo(1)–O(5)–Mo(4a)	115.8 (4)	Mo(3)–O(9)–Mo(4)	117.1 (6)
Mo(1)–O6–Mo(4a)	115.6 (5)	Mo(2)–O(8)–Mo(4a)	117.3 (6)

Table VI. 40.66-MHz ^{17}O NMR Data for Hexanuclear Poly Oxomolybdate Complexes of the General Type [(Mo$_5$O$_{18}$)X]$^{n-}$ (X = −MoO, −Ti(C$_5$H$_5$), and −Mo(NNC$_6$F$_5$) and n = 2–, 3–, and 3–, Respectively)

complex	chem shift (assgnt) [line width]^{a,b}
[Mo$_6$O$_{19}$]$^{2-}$	−37 (O$_1$) [30], 565 (O$_2$) [74], 940 (O$_3$) [156]
[(Mo$_5$O$_{18}$)Ti(C$_5$H$_5$)]$^{3-}$	5 (O$_1$) [11], 516 and 535 (O$_2$, O$_3$) [43, 64], 541 (O$_4$) [49], 834 (O$_6$) [93], 863 (O$_5$) [130]
[(Mo$_5$O$_{18}$)Mo(NNC$_6$F$_5$)]$^{3-}$	29 (O$_1$) [125], 567 and 602 (O$_2$, O$_3$) [71, 137], 645 (O$_4$) [137], 914 (O$_6$) [196], 930 (O$_5$) [143]

^{a} Chemical shifts referred to H$_2$^{17}O in ppm. All peak widths at half-height are given in Hz. Spectra are recorded at 297 K. ^{b} Oxygen assignments refer to labeling scheme displayed for idealized structures in Figure 9.
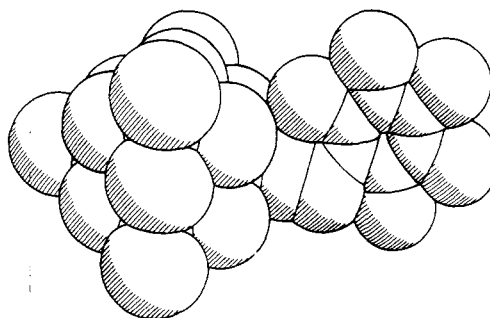
Figure 8. Structure of [Mo$_6$O$_{18}$(NNC$_6$F$_5$)]$^{3-}$ shown as a space-filling model where oxygen centers are drawn as shaded spheres with van der Waals radii of 1.4 Å.
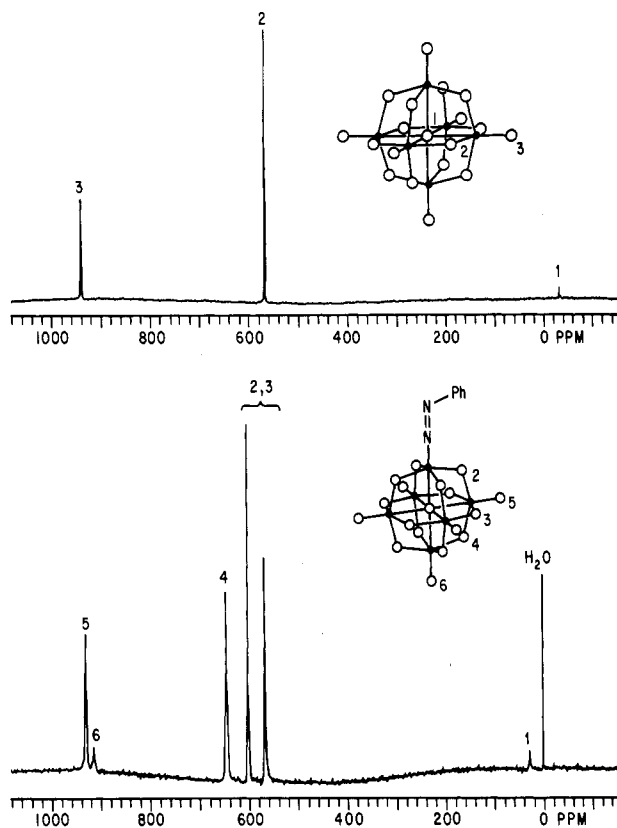
be described as a cubic close-packed arrangement of oxide anions, with one O^{2-} replaced by the diazenido ligand −NNC$_6$F$_5$$^+$, as shown in Figure 8.

The structural parameters for the Mo–NNC$_6$F$_5$ unit are consistent with the description of the (pentafluorophenyl)diazenido linkage as the three-electron donor species −NNR$^+$, a formalism that considers the diazenido ligand as isoelectronic with the nitrosyl group −NO$^+$ in its more common coordination mode.[26] One consequence of this description in the assignment of the formal oxidation state of Mo(1) as +2. In this sense, [(Mo$_5$O$_{18}$)Mo-(NNC$_6$H$_5$)]$^{3-}$ may be viewed as directly analogous to the [(Mo$_5$O$_{18}$)Ti(C$_5$H$_5$)]$^{2-}$ anion, with a [Mo(NNC$_6$F$_5$)]$^{3+}$ unit replacing the [Ti^{IV}(C$_5$H$_5$)]$^{3+}$ group of the latter structure.

^{17}**O NMR Spectrum of [n-Bu$_4$N]$_3$[Mo$_6$O$_{18}$(NNC$_6$F$_5$)].** [n-Bu$_4$N]$_3$[Mo$_6$O$_{18}$(NNC$_6$F$_5$)] displays the completely resolved ^{17}O NMR spectrum shown in Figure 9 with spectral data listed in
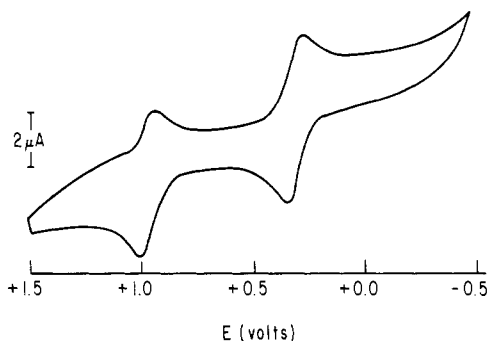
(26) Sutton, D. *Chem. Soc. Rev.* **1975**, *4*, 443.

Figure 9. Top: Idealized bond structure of $[Mo_6O_{19}]^{2-}$, with one member from each set of equivalent oxygen atoms labeled, and the ^{17}O NMR spectrum of $[Mo_6O_{19}]^{2-}$. Bottom: Idealized bond structure of $[Mo_6O_{18}(NNC_6F_5)]^{3-}$, with one member from each set of equivalent oxygen atoms labeled, and the ^{17}O NMR spectrum.

Table VI, where the resonances are assigned to chemically non-equivalent oxygen types by comparison with chemical shift data for $[Mo_6O_{19}]^{2-}$ and $[(Mo_5O_{18})Ti(C_5H_5)]^{3-}$. The assignment is based on the observed correlation between ^{17}O chemical shifts and Mo(VI)–O bond lengths.[27,28] In general, the longer the Mo–O bond distance, the greater the negative charge on the oxygen atom and the greater shift to higher shielding. The resonance at 29 ppm is thus assigned to the central oxygen, labeled 1 in the spectrum. The resonances at 914 and 930 ppm are assigned to the terminal oxo groups, of types 6 and 5, respectively. The upfield position of the resonance assigned to the unique MoO terminal oxygen is a direct consequence of the trans bond alternation discussed above, which predicts that the local increase in the negative surface charge produced by replacement of an $[Mo^{VI}O]^{4+}$ unit in $[Mo_6O_{19}]^{2-}$ by the $[Mo^{II}(NNC_6F_5)]^{3+}$ unit of $[Mo_6O_{18}(NNC_6F_5)]^{3-}$ is delocalized to the distal type 6 oxygen to a greater extent than to the proximal type 5 oxygens. This effect is entirely analogous to that observed for $[(Mo_5O_{18})Ti(C_6H_5)]^{3-}$. The assignment of the bridging oxygen resonances cannot be made totally unambiguously. By comparison to $[(Mo_5O_{18})Ti(C_6H_5)]^{3-}$, the 645 ppm resonance is assigned to Mo(1)–O–Mo bridging oxygens, while the 602 and 567 ppm resonances for the two nonequivalent Mo–O–Mo oxygen sets are not assigned to individual oxygens.

Electrochemical and EPR Studies of $[Mo_6O_{18}(NNR)]^{3-/2-}$ Complexes. Of the complexes of poly oxomolybdate anions with organohydrazine ligands, only the hexanuclear species $[Mo_6O_{18}(NNR)]^{3-}$ display well-behaved and reversible electrochemical behavior. This observation is consistent with the reversibility of redox processes associated with type I polyanion structures, those with a single terminal oxo group per metal.[29]

(27) Filowitz, M.; Ho, R. K. C.; Klemperer, W. G.; Shum, W. *Inorg. Chem.* **1979**, *18*, 93. Filowitz, M.; Klemperer, W. G.; Messerle, L.; Shum, W. *J. Am. Chem. Soc.* **1976**, *98*, 2345.

(28) Freeman, M. A.; Schultz, F. A.; Reilley, C. N. *Inorg. Chem.* **1982**, *21*, 576.

Figure 10. Cyclic voltammogram of $[Mo_6O_{18}(NNC_6F_5)]^{3-}$. Conditions: standard three-electrode configuration with a Pt-bead working electrode; solution 5×10^{-3} M in complex in CH_3CN, with 0.2 M $[n\text{-}Bu_4N][PF_6]$ as supporting electrolyte.

Table VII. Summary of Cyclic Voltammetric Data[a] for Hexanuclear Oxomolybdate Complexes

complex	$E_{1/2}$, V^b	WE_p, mV	i_p^f/ i_p^{rc}	$i_p/Cv^{1/2}$, mA $s^{1/2}$ mV$^{-1/2 d}$	n
$[Mo_6O_{19}]^{2-}$	−0.82	61	1.0	8.4	1.0
	−1.68	82	2.4	9.0	1.3
$[Mo_6O_{18}(NNC_6H_4\text{-}p\text{-}OCH_3)]^{3-}$	−0.02	62	1.0	8.4	1.0
	+0.71	93	1.9	8.5	1.0
$[Mo_6O_{18}(NNC_6H_5)]^{3-}$	+0.06	60	1.0	8.5	1.0
	+0.82	88	1.6	8.7	1.0
$[Mo_6O_{18}(NNC_6H_4\text{-}p\text{-}NO_2)]^{3-}$	+0.14	60	1.0	8.6	1.0
	+0.95	79	1.6	8.6	1.0
$[Mo_6O_{18}(NNC_6F_5)]^{3-}$	+0.30	61	1.0	8.4	1.0
	+1.0	87	1.8	8.6	1.0

[a] Cyclic voltammograms were carried out in methylene chloride, 1.0 $\times 10^{-3}$ M in complex and 0.2 M in $[Bu_4N][PF_6]$ at a platinum working electrode, by using a sweep rate of 250 mV s^{-1}. [b] Estimated by cyclic voltammetry from $E_{1/2} = (E_p^f - E_p^r)/2 = E_p - 29$ mV. The shape parameter $E_p^f - E_{p/2}$ lay within the range 60–80 mV for the initial electrode process in all cases. [c] Peak current ratio at 250 mV s^{-1}. [d] The current function was close to that observed for the ferrocene–ferrocenium couple at the same electrode (8.5 mA s$^{1/2}$ mV$^{-1/2}$).

However, in contrast to other examples of type I polyanions, which display reversible reductions exclusively, the $[Mo_6O_{18}(NNR)]^{3-}$ class of derivatized polyanions exhibits reversible oxidative processes. While $[Mo_6O_{18}(NNR)]^{3-}$ represents a member of the type I structures, all other organohydrazido derivatives of this study are classified as type II structures and are characterized by irreversible multielectron cathodic processes at large negative potentials.

A cyclic voltammogram for $[Mo_6O_{18}(NNC_6H_5)]^{3-}$ is shown in Figure 10, and the relevant electrochemial data are presented in Table VII. In contrast to the electrochemical behavior of $[Mo_6O_{19}]^{2-}$, which displays two successive one-electron cathodic processes,[30] the cyclic voltammograms of diazenido derivatives $[Mo_6O_{18}(NNR)]^{3-}$ are characterized by two successive one-electron oxidative processes:

$$[Mo_6O_{18}(NNR)]^{3-} \xrightarrow{-e^-} [Mo_6O_{18}(NNR)]^{2-} \xrightarrow{-e^-}$$
$$[Mo_6O_{18}(NNR)]^-$$
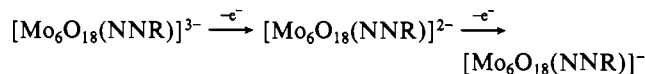
While the first anodic process conforms to the criteria for Nernstian reversibility, the succeeding oxidation is irreversible, even at scan rates of 30 V s^{-1}, indicating a fast following chemical reaction of the monoanion.

No cathodic processes were observed for $[Mo_6O_{18}(NNR)]^{3-}$ complexes at potentials up to −2.4 V in acetonitrile, DMF, or CH_2Cl_2, indicating that the lowest unoccupied molecular orbital (LUMO) is at least 60 kcal higher in energy than the highest occupied molecular orbital (HOMO) of the diazenido derivatives.

(29) Pope, M. T. In *Heteropoly and Isopoly Oxometalates*; Springer: New York, 1983.

(30) Che, M.; Fournier, M.; Launay, J. P. *J. Chem. Phys.* **1979**, *71*, 1954.
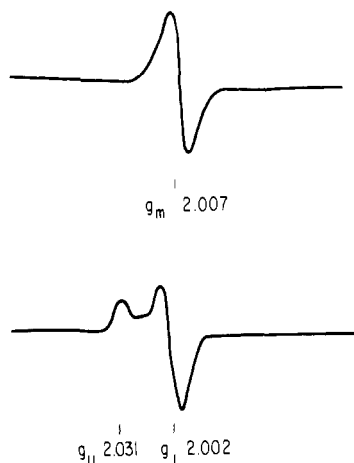
Figure 11. EPR spectra of $[Mo_6O_{18}(NNC_6H_5)]^{3-}$ in DMF, recorded at (top) 277 K and (bottom) 77 K.

The relatively facile reduction of $[Mo_6O_{19}]^{2-}$ to $[Mo_6O_{19}]^{3-}$ has been ascribed to the availability of a LUMO of essentially non-bonding character, which results in minimal bond length alternation upon reduction.[31] In contrast, the LUMO of the diazenido derivatives must be destabilized by at least 40 kcal relative to that of $[Mo_6O_{19}]^{2-}$. Thus, the redox activity of the $[Mo_6O_{18}(NNR)]^{3-}$ derivatives is attributed to the accessibility of the HOMO, an orbital that is associated with the metal–diazenido interaction for mononuclear molybdenum–diazenido complexes.[32]

In an effort to establish the nature of the orbital involved in the oxidative processes displayed by the $[Mo_6O_{18}(NNR)]^{3-}$ complex, controlled-potential electrolysis was performed on samples of $[Mo_6O_{18}(NNR)]^{3-}$. At the end of 1 faraday mol^{-1} electrooxidation at +0.45 V, EPR spectra of $[Mo_6O_{18}(NNR)]^{2-}$ were recorded at 4 and −196 °C, as shown in Figure 11. In contrast to the spectrum of the reduced-form species $[Mo_6O_{19}]^{3-}$, the EPR spectrum of $[Mo_6O_{18}(NNR)]^{2-}$ displays no molybdenum hyperfine lines, even at −196 °C. This observation is consistent with a redox process centered at a molybdenum center with an oxidation state other than +5, such as the Mo(1) center of these derivatives, or, alternatively, delocalization of the unpaired electron in the cluster, even at low temperatures. The sensitivity of the oxidation potentials to the substituents on the diazenido ligand (NNR), shown in Table VII, is consistent with the unpaired electron primarily localized on the diazenido unit. In either case, the temperature-dependent hopping mechanism invoked to explain the appearance of Mo-hyperfine coupling in $[Mo_6O_{19}]^{3-}$[30,31] does not appear to be applicable in this instance. This observation establishes that replacement of the $[Mo^{VI}O_t]^{4+}$ unit by the $[Mo^{II}(NNR)]^{3+}$ fragment effects profound changes in the electronic distribution of the complex, which may in turn perturb the ^{95}Mo NMR spectra of these species (vide infra). The value of g for the solution spectrum of 2.010 is similar to those observed for other Mo–diazenido complexes,[32] while the axial spectrum, $g_\parallel = 2.089$ and $g_\perp = 1.999$, observed at low temperature, is consistent with axial geometry of a C_4 local symmetry complex, $[Mo_6O_{18}(NNR)]^{2-}$. In contrast to $[Mo_6O_{18}(NNR)]^{3-}$, mononuclear Mo–diazenido complexes display well-resolved molybdenum hyperfine lines.[32]

The electrooxidation is accompanied by a dramatic color change from pale orange-brown for $[Mo_6O_{18}(NNR)]^{3-}$ to an intense violet for the oxidized species. This change may be monitored in the electronic spectrum by the disappearance of the band at ca. 390 nm and the appearance of a band at 439 nm. The intensities of the transitions in both the reduced and oxidized forms $[Mo_6O_{18}(NNR)]^{3-/2-}$ indicate that these are charge-transfer bands. Since the positions of the bands are independent of solvent

(31) Sanchez, C.; Livage, J.; Launay, J. P.; Fournier, M.; Jeannin, Y. *J. Am. Chem. Soc.* **1982**, *104*, 3194.
(32) Butler, G.; Chatt, J.; Leigh, G. J.; Pickett, C. J. *J. Chem. Soc., Dalton Trans.* **1979**, 113.

Table VIII. Comparison of Molybdenum–Oxygen Distances for Selected Compounds

		$[Mo_6O_{18}(NNC_6F_5)]^{3-}$	
	$[Mo_6O_{19}]^{2-}$	$Mo_2-Mo_6{}^b$	$Mo_1{}^c$
Mo–O$_c{}^a$	2.318 (5)	2.36 (1)	2.19 (1)
Mo–O$_b$	1.925 (7)	1.95 (1)	2.00 (1)
		1.88 (1)	
Mo–O$_t$	1.677 (5)	1.69 (1)	

^{a}Abbreviations: O$_c$, central oxygen; O$_b$, bridging oxygen atoms; O$_t$, terminal oxygen atoms. ^{b}Mo sites coordinated to oxygen atoms only, MoO$_6$ sites. ^{c}Mo site bonded to the diazenido ligand, MoO$_5$N site.

(CH$_3$CN, DMF, CH$_2$Cl$_2$), the processes are intramolecular. Whereas the unsubstituted poly oxomolybdate $[Mo_6O_{19}]^{2-}$ is pale yellow and shows no charge-transfer bands in the 300–600-nm region, the $[Mo_6O_{18}(NNR)]^{3-}$ complexes are orange-brown, suggesting that the 390- and 523-nm bands are charge-transfer transitions located within the Mo–N–NR chromophore. The bathochromic shift from 390 to ca. 425 nm upon oxidation is consistent with a process involving an orbital of predominantly metal–diazenido π-bonding character.

The intimate involvement of the metal–diazenido center in the anodic process is further demonstrated by the substituent effects. The primary oxidation potentials show the expected trends: the more electron withdrawing the substituents, the more positive the oxidation potential or the lower the energy of the HOMO.

Discussion

The observation that the absence of the molybdenum signal at 292 K for $[Mo_8O_{26}]^{4-}$ is due to line width rather than any fluxional behavior is fully consistent with the results of ^{17}O NMR studies for this compound. The number of ^{17}O and now ^{95}Mo signals precludes exchange on the NMR time scale. That the signals have very different line widths is likely related to the differing quadrupolar coupling constants for the sites of differing symmetries. Although one of the sites is tetrahedral and the other is octahedral, the structure of the compound does not reveal any large differences in site symmetry.

For quadrupolar nuclei such as molybdenum, sites of moderately differing symmetries can lead to substantially differing quadrupolar coupling constants. Since the line width depends upon the quadrupolar coupling constant and is temperature dependent, the absence of an expected signal may be the result of substantial broadening.

In spite of this potential problem for quadrupolar nuclei, the data in Table I reveal that for the most part the expected number of ^{95}Mo NMR signals are seen in the spectra of the compounds under study. Moreover, the chemical shift range of the signals and the line widths are fully consistent with oxomolybdates of Mo(VI). For those that had fewer signals than expected, either temperature variation produced no change in the number of signals ($[Mo_4O_{11}(O)(hydralazine)]^{2-}$ (anion of **7**)) and $[Mo_8O_{16}(OMe)_6(N_2PhMe)_6]^{2-}$ (anion of **9**)) or the change was irreversible ($[Mo_6O_{18}(NNPh)]^{3-}$ (anion of **10**)).

Nevertheless, the data indicate that simple correlations of structure and chemical shift may have difficulties. This is illustrated in several ways, first by noting the enormous changes brought about by a single terminal oxygen substitution and second by comparing chemical shift values for the same structural fragments in differing compounds.

The complex $[Mo_6O_{19}]^{2-}$ has a single octahedral molybdenum site with five bridging oxygens and one terminal oxygen. The ^{95}Mo signal at 126 ppm for this compound is in fact the least shielded molybdate signal known. Replacement of a single terminal oxygen by the phenyldiazenido group leads to the complex $[Mo_6O_{18}(NNPh)]^{3-}$ (anion of **10**), whose gross structure is the same as that of $[Mo_6O_{19}]^{2-}$. However the ^{95}Mo NMR spectrum of this compound displays two signals of differing line widths at −57.9 and −23.9 ppm, respectively. At least one of these signals must be assigned to a molybdenum center with a terminal oxo substituent, and whichever that is the change in chemical shift from the unsubstituted is enormous.

Thus, while the gross structure is the same, the electron density at the molybdenum atoms as revealed by chemical shift is greatly affected. Inspection of the several Mo–O distances for the two compounds (Table VIII) reveals significant differences. Most notably, substantial increases and decreases are seen for molybdenum to bridging and connecting oxygen bonding distances whereas molybdenum to terminal oxygen distances are essentially the same. The transmission of the effect of the substituent variation to other molybdenum atoms via the oxygen bridges is noteworthy in the effects on bond distances, symmetry at sites, and chemical shift. Furthermore, the ligand influences may be substantial, in view of the "noninnocent" nature of the strongly π-bonding diazenido and hydrazido(2-) groups. It is established in mononuclear Mo(VI) complexes that replacement of an oxo group by a phenylimido group can deshield the ^{95}Mo nucleus by 140 ppm.[9] The sensitivity of the chemical shifts to the introduction of the nitrogenous ligand is not unanticipated nor is the transmission of the effect throughout the cluster sites. It may be argued that the diazenido-coordination centers are no longer Mo(VI) sites but Mo(II) or Mo(IV) sites depending upon the description of the diazenido group. In either case the electronic environment at the Mo centers is significantly perturbed from that of a oxomolybdate(VI) site, and a chemical shift variation is anticipated. The available ^{95}Mo NMR data confirm that formally Mo(II) mononuclear complexes display chemical shifts over a range greater than 4000 ppm (+2000 to −2100 ppm).[33,34] Compounds containing the [MoNO]$^{3+}$ moiety, which is electronically analogous to the [MoNNR]$^{3+}$ unit of [Mo$_6$O$_{18}$(NNPh)]$^{3-}$, display a chemical shift range of 0–2200 ppm. The chemical shift depends upon current density and not upon charge density, and it is not clear how a metal such as ^{95}Mo will change its chemical shielding with either current or charge density. The reason for this uncertainty is that the metal is a relativistic metal, i.e. one dominated by spin–orbit effects in the presence of a magnetic field. While one result of this is the loss of correlation between seemingly isolated structural units and chemical shift charts, a second result is the great sensitivity of the NMR chemical shift to detailed structural changes.

The conclusion that there are enormous changes in bonding as revealed by chemical shift differences is supported by large differences in the electrochemistry and UV–visible absorption of the compounds. The charge-transfer band at 523 nm in [Mo$_6$O$_{18}$(NNAr)]$^{3-}$ is characteristic of the Mo–diazenido unit, while [Mo$_6$O$_{19}$]$^{2-}$ presents no transitions in the visible region. The consequences of diazenido coordination are also evident in the contrasting electrochemical characteristics: [Mo$_6$O$_{19}$]$^{2-}$ displays a one-electron reduction at −0.8 V, while [Mo$_6$O$_{18}$(NNAr)]$^{3-}$ displays a reversible one-electron oxidation in the range 0.0 to +0.3 V, depending upon the substituent.

The lack of simple correlation between the structural units in a given compound and some consistent chemical shift value that could be assigned to that unit is revealed in Table II. In the table the probable chemical shift value for tetrahedral and octahedral molybdenum atoms with varying bridging and terminal oxygens are tabulated. Focusing attention on tetrahedral molybdenum atoms with two bridging and two terminal oxygens, one can assign chemical shift values of −60, −18, and +20 ppm from select compounds. Similarly, for tetrahedral molybdenum with one terminal oxygen and three bridging oxygens, chemical shift values of −60, −24, and +24 ppm are probable. Moreover the gross structures of the compounds provide no obvious reason for such a significant chemical shift variation. What emerges is that a given structural unit does not give rise to a signal in a characteristic range but that in some nonobvious way the chemical shift markedly depends upon more remote substitutions.

Thus, the use of chemical shift correlations to assign structural units, which finds such great utility in ^{13}C NMR spectroscopy, is largely absent in ^{95}Mo NMR spectroscopy in these complexes, and one has to proceed with far greater caution. However, such correlations are observed in well-defined simpler structures. This suggests that the molybdenum NMR shifts of the complexes in this study are more sensitive to changes at positions that would be considered remote in carbon NMR spectroscopy. One wonders how much of this is the result of an enhanced transmission (via the shared oxygens) of electronic perturbations and how much is inherent in the molybdenum quadrupolar nucleus. Some amplification of these considerations follows.

Consider a delocalized bonding scheme that in turn leads to a delocalized current density over a sphere—in this case the cluster molecule. When that situation is perturbed, there is a redistribution of current density over the surface of the sphere; i.e., the bonding is perturbed in such a way as to cause the current density to localize at a particular center or region. Moreover, doing so lowers the symmetry. Both effects could have significant effects on the shielding of the various atoms but only have minor effects on the overall gross structure of the molecule. Alternatively, the substituent might not perturb the overall electron or current density in the molecule but simply lower the symmetry. This now allows much more mixing of states and could cause significant chemical shifts.

Supplementary Material Available: Tabulated experimental details for the X-ray diffraction study of [*n*-Bu$_4$N]$_3$[Mo$_6$O$_{18}$(NNC$_6$F$_5$)], interatomic distances and angles, and hydrogen atom positional and thermal parameters (8 pages); tabulated calculated and observed structure factors (12 pages). Ordering information is given on any current masthead page.

(33) Minelli, M.; Enemark, J. H.; Brownlee, R. T. C.; O'Connor, M. J.; Wedd, A. G. *Coord. Chem. Rev.* **1985**, *68*, 169.

(34) Young, C. G.; Minelli, M.; Enemark, J. H.; Hussain, W.; Jones, C. J.; McCleverty, J. A. *J. Chem. Soc., Dalton Trans.* **1987**, 619.